Journal of Alloys and Compounds 509 (2011) 5701–5707

Contents lists available at ScienceDirect

Journal of Alloys and Compounds

journal homepage: www.elsevier.com/locate/jallcom

High frequency response to the impedance complex properties of Nb-doped $CaCu_3Ti_4O_{12}$ electroceramics

Muhammad Azwadi Sulaiman[a], Sabar D. Hutagalung[a,*], Julie J. Mohamed[a], Zainal A. Ahmad[a], Mohd Fadzil Ain[b], Bakar Ismail[c]

[a] School of Materials and Mineral Resources Engineering, Universiti Sains Malaysia, 14300 Nibong Tebal, Penang, Malaysia
[b] School of Electrical and Electronic Engineering, Universiti Sains Malaysia, 14300 Nibong Tebal, Penang, Malaysia
[c] Physics Department, Faculty of Science, Universiti Teknologi Malaysia, 81310 Skudai, Johor, Malaysia

ARTICLE INFO

Article history:
Received 25 September 2010
Received in revised form 22 February 2011
Accepted 24 February 2011
Available online 4 March 2011

Keywords:
Powders-solid state reaction
Grain boundaries
Dielectric properties
Impedance
Perovskites

ABSTRACT

Impedance analyses was performed on undoped and Nb-doped $CaCu_3Ti_4O_{12}$ ($CaCu_3Ti_{4-x}Nb_xO_{12+x/2}$; $x = 0$, 0.01, 0.03, 0.05, 0.1) to investigate their electrical properties. The pellet samples were prepared using the solid state reaction method. Silver electrode was deposited on both pellets' surfaces for electrical measurement. The thermally etched samples showed tiny bumped domains within the grains. The existence of both domain and grain boundaries are believed to strongly influence the dielectric constant of $CaCu_3Ti_4O_{12}$ (CCTO). Undoped CCTO showed two arcs of impedance complex plane while Nb-doped samples have three arcs. Each arc represents the constituent elements of the CCTO. The highest frequency arc is evidence that CCTO consists of conductive domains which measure about 1 Ω and are insulated by two types of barriers, i.e. domain boundary and grain boundary.

1. Introduction

Nowadays, $CaCu_3Ti_4O_{12}$ (CCTO) has attracted much attention of researchers due to its giant dielectric constant behavior [1,2]. It can achieve 100,000 at room temperature and has very small temperature dependence in a wide temperature range, from 100 to 400 K. This high dielectric constant material has good potential for application in the process of miniaturized electronic and microelectronic devices such as capacitors, resonators and filters. The origin of the giant dielectric constant of CCTO is still an on-going discussion among researchers. Some models and mechanisms were proposed such as (1) electrode polarization effects or surface layer effect [3,4], (2) internal barrier layer capacitor (IBLC) [5,6], (3) fluctuations of lattice distortion induced dipoles in nanosize domains [7], and (4) intra-granular network [8].

Impedance spectroscopy (IS) has become essential in electrical characterization of ceramic materials. This IS technique assumes that the properties of the electrode and material system are time-invariant, thus one of the basic uses of IS is to determine the interrelations and dependences of desired controllable variables such as temperature, applied static voltage and current bias. Oliver Heaviside in the 1880s introduced the concept of electrical impedance which later developed in terms of vector diagrams and complex representations by other researchers [9]. The concept was applied for microstructural analyses of polycrystalline materials. Recently, higher and wider frequency ranges of impedance complex plane measurements have motivated reseachers into better understanding their subjected materials.

In polycrystalline solids, the electrical properties of constituent phase are strongly affected by microstructure and impedance spectra which commonly represent features that can be directly related to the microstructure. Different phases also exhibit different responses when applying certain alternating signals. IS was developed as a technique to illustrate these responses in the form of valuable plotting functions. By combining more than one response, it is possible to model and describe microstructure elements, usually grains and grain boundaries of differing phase compositions, suspension of one phase within another, and porosity.

Many impedance models have been proposed based on IS measurements for various types of microstructures. One of them is the internal barrier layer capacitor model or brick layer capacitor which is usually found on structures of dielectric ceramic. The internal barrier layer capacitor model is based on limited reoxidation of a reduced composition and results in higher resistivity of the surface layer than in a central portion [10]. A thinner reoxidized layer will produce larger dielectric ceramic permittivity [11,12]. A modified model structure is illustrated in Fig. 1(a). The capacitance, C_i of an

* Corresponding author. Tel.: +60 4 5996171; fax: +60 4 5941011.
E-mail address: mrsabar@eng.usm.my (S.D. Hutagalung).

0925-8388/$ – see front matter © 2011 Elsevier B.V. All rights reserved.
doi:10.1016/j.jallcom.2011.02.145

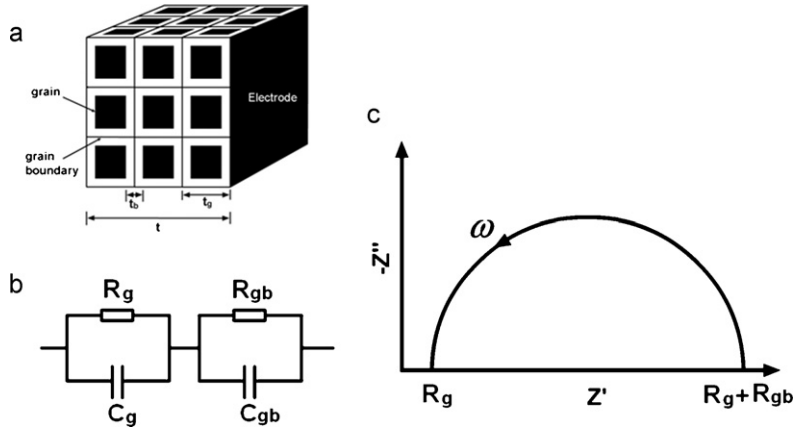

Fig. 1. The grain and grain boundary structure model (brick-layer model) (a), an equivalence circuit of two sets of parallel resistor and capacitor (b), and schematic of impedance complex plane plot (c).

individual element is given by

$$C_i = \frac{\varepsilon_r \varepsilon_o t_g^2}{t_b} \quad (1)$$

and that of a series connected column by

$$\frac{C_i}{\text{no. of elements in column}} = \frac{\varepsilon_r \varepsilon_o t_g^2 / t_b}{t/t_b} \quad (2)$$

The t_b is grain size while t_g is grain boundary thickness.

The capacitance per unit area is

$$C = \frac{\varepsilon_r \varepsilon_o t_g}{t t_b} \quad (3)$$

Since there are $1/t_g^2$ columns per unit area, it follows that the effective relative permittivity, ε_{re} of the composite dielectric is

$$\varepsilon_{re} = \frac{\varepsilon_r t_g}{t_b} \quad (4)$$

Higher resistivity in grain boundary or barrier layer than in the inner side of grains in many polycrystalline dielectric ceramics can be demonstrated as an equivalence circuit of two sets of parallel resistors and capacitors known as *RC* elements which are connected in a series as shown in Fig. 1(b). The R_g and R_{gb} are resistivity of grain and grain boundary respectively, while C_g and C_{gb} are capacitance of grain and grain boundary, respectively. The two *RC* elements connected in a series respond at different relaxation time constants leading to the formation of a semicircle as shown in Fig. 1(c). The separate responses may overlap and the experimental curve must then be resolved into separate constituent semicircles.

Some of the common plotting functions in ceramic electrical characterization are impedance complex plane, dielectric constant and dielectric loss versus frequency. In current CCTO studies, researchers lack high frequency measurements in their investigations. In addition to this, many electronic application standards nowadays, especially for the communication industry, operate at above high frequency radio waves (>3 MHz) [13]. Such applications require dielectric material with a capability to withstand high dielectric constants at high frequencies. As an example, the dimension multiples of a dielectric resonator antenna (DRA) can be reduced by increasing the ε of its dielectric material [14].

Many methods can be used to improve dielectric constant, decrease the overall dielectric loss and alter the resonant effect of CCTO. These methods include substitution, doping and two-phase composite processes [15–19]. Hong et al. [16] investigated Nb doped CCTO from 0.01 Hz to 1 MHz of frequency and found out that the highest dielectric constant is ~420,000 at 10 kHz and dielectric loss is lower than 1 at <0.1 mol% over the frequency range. Liu et al. [20] reported the electrical properties of Nb doped CCTO from 40 Hz to 110 MHz which is a higher frequency range than that used by Hong et al. [16]. The literature indicates that increasing the concentration of Nb doping to 0.2 mol% will lower the dielectric loss to below 3 in the range of 1–110 MHz of frequency.

The electrical properties in the high to very high frequency range actually have not been much reported. In this study, IS was used to investigate the Nb doped CCTO impedance from low to very high frequencies of 1 Hz to 1 GHz. In our previous report [21], it was shown that introducing Nb dopant into CCTO can exponentially reduce the dielectric loss of undoped CCTO from 1.5 to about 0.3 for 0.1 mol% at 1 MHz which is lower than Hong et al.'s [16] finding. According to the report, the low dielectric loss produced by high Nb concentrations in CCTO is only until 20 MHz, after which the dielectric loss of undoped CCTO is lower. As observed in previous literature, donor dopants other than Nb show increase of dielectric loss with dopant addition at 1 MHz, for example, La doped CCTO and Cr doped CCTO [22,23].

The enhancement of dielectric constant without affecting the dielectric loss of Nb-doped CCTO is a very interesting phenomenon and as mentioned before, the key to understanding material–electrical relations is through impedance complex plane analyses. Hong et al. [16] reported that a semicircle arc with curve fitting plot indicates a reduction of grain boundary resistivity with increased Nb content. Liu et al. [20] who measured IS on a wider frequency range also found the same arc with an extra arc at low frequency and another small incomplete arc at very high frequency. The literature suggests that there are three arcs which represent three *RC* elements which originate from the polarization response of elements inside CCTO. Shao et al. [24] have also suggested that another semicircle must exist at an upper frequency region which is beyond the frequency measurement range when observing at room temperature and that this semicircle is a contribution of domain resistance. The literature also considers that CCTO ceramic contains conducting domains and two kinds of insulating barriers, i.e. domain boundaries and grain boundaries. Fang et al. [25] also agree that there are three semicircles in CCTO and one of them is present at high frequency but was not revealed in their measurement.

2. Experimental procedures

The solid state reaction method was used to produce undoped and Nb-doped CCTO ceramics. The same method used in the previous report for $CaCu_3Ti_4O_{12}$ (CCTO) preparation was adopted [26–28]. The raw materials for $CaCO_3$, CuO and TiO_2 were firstly weighted according to the stoichiometric ratio for undoped CCTO. The raw materials were then mixed via ball milling process for 1 h using an alumina jar. Zirconia balls were used as the grinding media with mass ratio of balls to raw materials of 10:1. The same steps were employed to produce Nb-doped CCTO, but with additions of 1, 3, 5 and 10 mol% of Nb from Nb_2O_5, respectively. The well

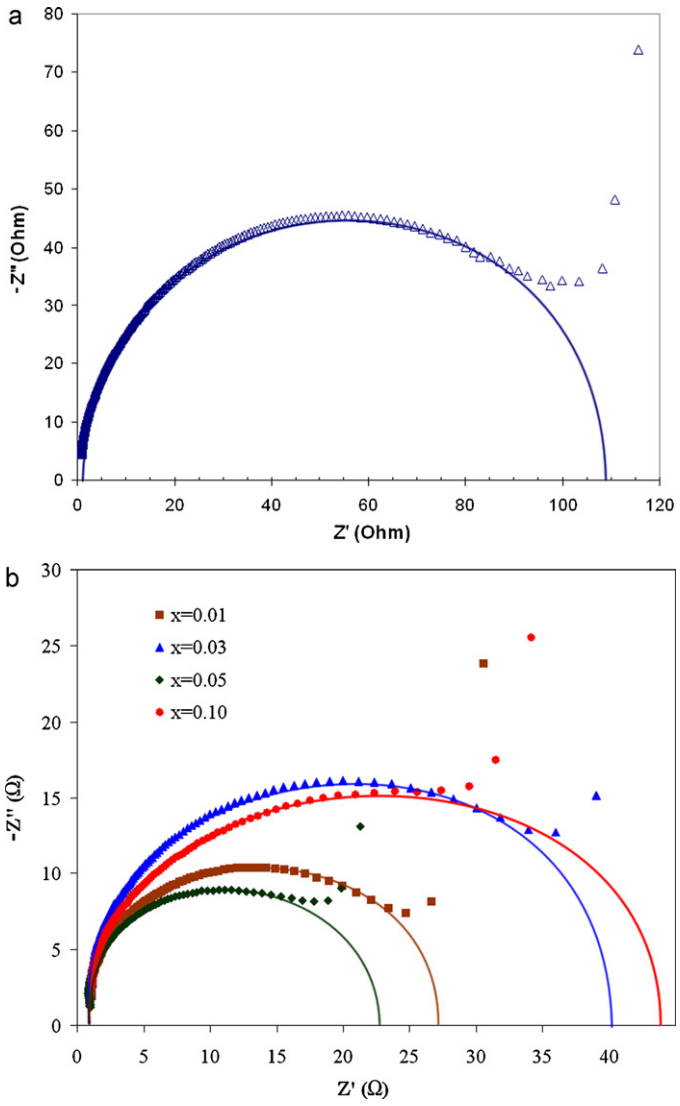

Fig. 2. Impedance complex plane plots for (a) undoped CCTO and (b) Nb-doped CCTOs ($CaCu_3Ti_{4-x}Nb_xO_{12+x/2}$) measured from 1 MHz to 1 GHz.

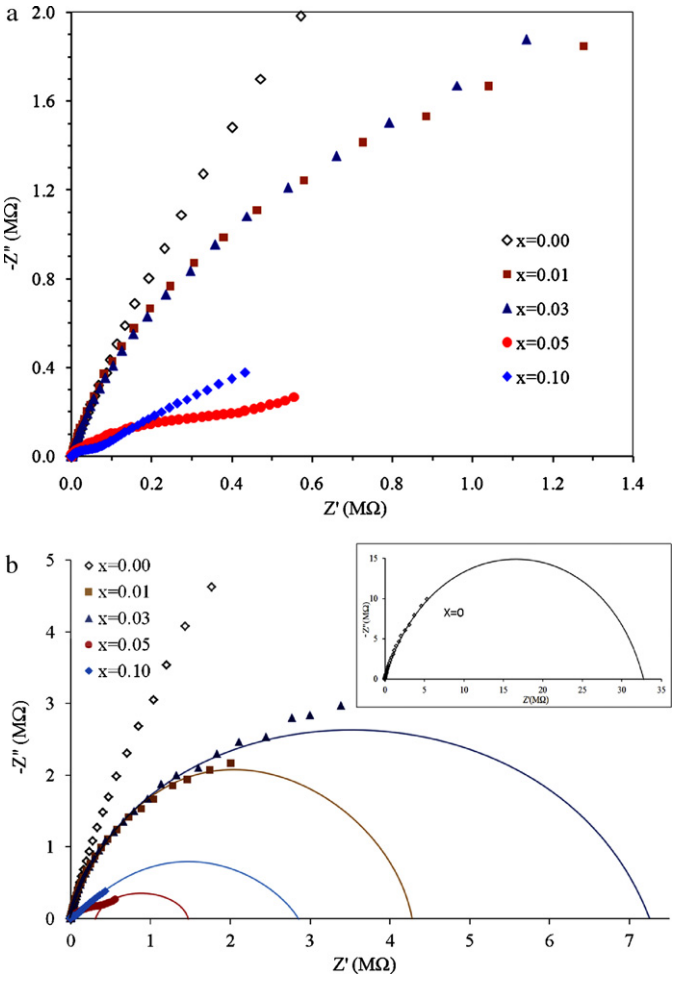

Fig. 3. (a) Impedance complex plane plots of $CaCu_3Ti_{4-x}Nb_xO_{12+x/2}$ measured from 1 Hz to 1 MHz, and (b) the numerical fitting of the impedance complex plane.

mixed raw material was calcined in air at 900 °C for 12 h in an alumina crucible. The calcined powder was pressed into pellet forms with a diameter of 12 mm and thickness of 3 mm using a hydraulic press at 350 MPa. The pellets were sintered in air at 1040 °C for 10 h and cooled naturally to room temperature.

Both pellet surfaces were polished and coated with silver paste as electrodes. Impedance complex plane measurement of CCTO was carried out using the Autolab Potentiostat (PGSTAT30) over a frequency range of 1 Hz to 1 MHz and the RF Impedance/Material Analyser 4291B Hewlett Packard was used for a range of 1 MHz to 1 GHz. The microstructures analysis by field-emission scanning electron microscopy (FESEM) Zeiss SUPRA 35VP was performed to selected pre-sintered $CaCu_3Ti_{4-x}Nb_xO_{12+x/2}$ pellets etched at 940 °C for 1 h.

3. Results and discussion

In order to understand the mechanism of the giant dielectric constant in CCTO, Sinclair et al. [5] applied a previously used concept of the brick layer model and testified it as an internal barrier layer capacitance (IBLC) which is also based on impedance spectroscopy (IS) measurements. IBLC focuses more on the first model from the general brick layer model by considering three possibilities: (1) insulative layer and conductive grain interior, (2) conductive layer and insulative grain interior and (3) combination of the two models [9]. In other words, it was suggested that CCTO is electrically heterogeneous. The semiconducting grain reacts with insulating grain boundary producing an intrinsic electrostatic barrier at grain boundaries surface. This can be illustrated as an electrical circuit with two parallel *RC* elements connected in a series. One of the *RC* elements represents the semiconducting grain, R_gC_b, and the other represents the insulating grain boundary, $R_{gb}C_{gb}$. This was proven by Chung et al. [29] using a combination of scanning Kelvin probe microscopy with a lateral bias and *I–V* measurement.

Fig. 2 shows a high frequency impedance complex plane of undoped and Nb-doped CCTO measured from 1 MHz to 1 GHz at room temperature. The low frequency impedance complex plane was also measured from 1 Hz to 1 MHz as shown in Fig. 3. In Fig. 2, it is shown that all samples indicated the presence of two arcs within the medium to high frequency range (1 MHz to 1 GHz) with non-zero intercepts. The high frequency arcs on the left can be a complete semicircle with a fitting curve and the other arcs are continuations from the low to medium frequency measurement. At the low to medium frequency range of 1 Hz to 1 MHz (Fig. 3), we found that the samples $x = 0.00$, 0.01 and 0.03 showed only one arc while the samples $x = 0.05$ and 0.10 showed two arcs. The combination of these two frequency ranges is a new wide range frequency measurement, i.e. 1 Hz to 1 GHz. Fig. 4 shows the impedance complex plane plots for the various $CaCu_3Ti_{4-x}Nb_xO_{12+x/2}$ samples in the wide range frequency of 1 Hz to 1 GHz. Based on the combination results, we can conclude that $CaCu_3Ti_{4-x}Nb_xO_{12+x/2}$ of $x = 0$, 0.01 and 0.03 has two arcs, while the remaining $x = 0.05$ and 0.1 has three arcs. These arcs can be extrapolated separately to become a com-

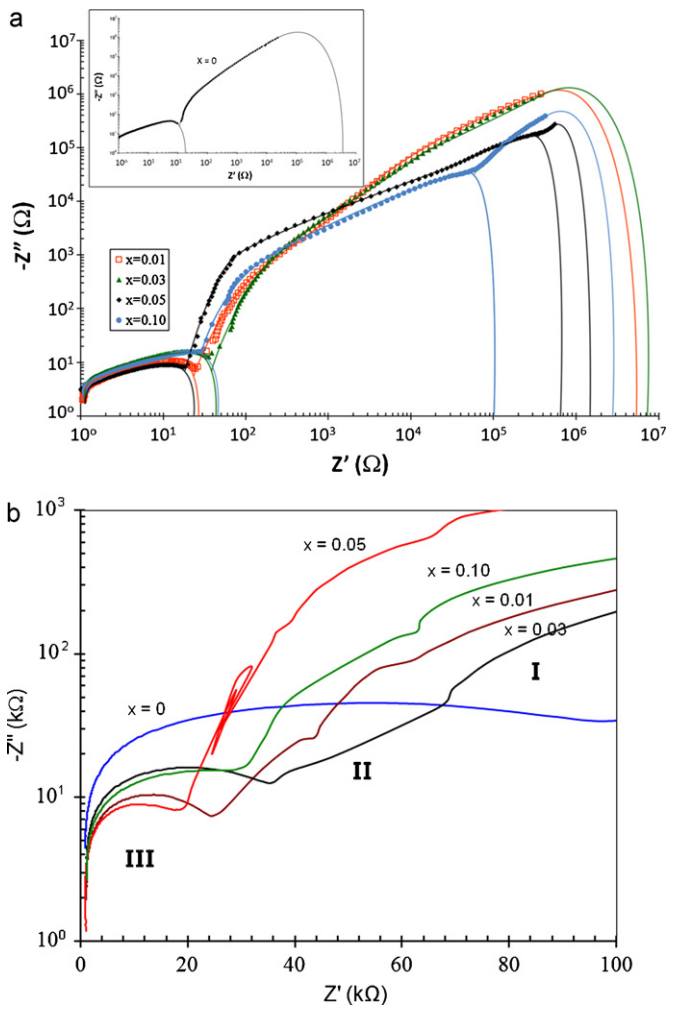

Fig. 4. Impedance complex plane plots of $CaCu_3Ti_{4-x}Nb_xO_{12+x/2}$ in the wide range frequency from 1 Hz to 1 GHz: (a) log–log graph, (b) semi-log graph on selected area.

plete semicircle which represents the resistance of each element (Fig. 4(a)).

Many researchers have reported that the CCTO only produces one or two arcs for the measured impedance complex plane [5,11,25,30–33]. These arcs can be easily detected at frequencies below 10 MHz. However, in this present work, we found three arcs (see Fig. 4(b)). In the case of the undoped CCTO sample, the additional arc starts to form from 8.5 MHz to 1 GHz to complete a semi-circular curve. Some literature which reported the impedance complex plane at the range of 40 Hz to 110 MHz found the small arc (the first arc from left at Fig. 4) at a higher frequency [20,24,34–36]. However, due to insufficient numerical data needed to complete the arc as a semi-circle, the discussion on high frequency arc was temporarily pended in the ideal equivalence circuit models.

The literatures also mention two models of impedance plots: the first using two arcs, and the second using three arcs [20,24,34–36]. The two arcs were modelled to an ideal equivalence circuit consisting of two parallel *RC* elements (R_gC_g and $R_{gb}C_{gb}$) while the three arcs consist of three *RC* elements (R_gC_g, $R_{gb}C_{gb}$ and R_xC_x) which are all connected in a series (Figs. 5 and 6). In our model which was based on a wide range of frequency, an additional *RC* element was included into the conventional models as a response of high frequency arc, instead of only low and medium frequencies [3,9,25,30–33]. Figs. 5(a) and 6(a) are the two and three arcs of the impedance complex plane model. Meanwhile, Figs. 5(b) and 6(b) are their ideal equivalence circuit with three and four *RC* elements,

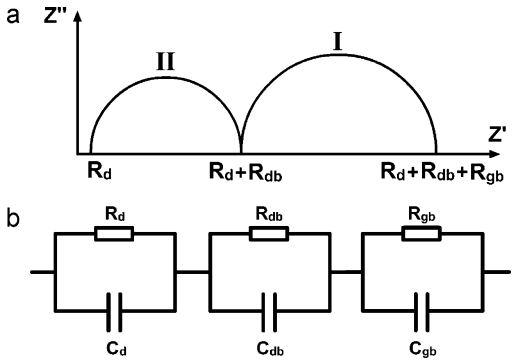

Fig. 5. Schematic impedance complex plane plot for two arc samples (a) and its equivalence *RC* circuit (b).

respectively. The three *RC* elements model shows that resistance at the medium frequency is originally a response from grain boundary resistance (R_{gb}) and resistance at high frequency is originally from domain (R_d) and domain boundary resistance (R_{db}). Meanwhile, the four *RC* elemental models obtained the R_xC_x element where R_x was identified as surface oxidation layer resistance at low frequency arcs [20,34,35].

Based on the microstructural model, the complex impedance simulated the brick-layer model with grain and grain boundary elements [9]. In our model, the micron size grain of CCTO might consist of submicron size or smaller grains, namely domains. The domains are separated from each other by domain boundaries to form domain arrays inside the grain. As a grouped domain, the grains are also separated by grain boundary. This proposed model was supported by SEM images of microstructure analysis which will be discussed later. The current flow is assumed to be one dimensional and the curvature of the current paths at the corners of the domains and grain is neglected. In case of CCTO, it is suggested that three paths are available to the current, as shown in Fig. 7. The current either passes through domains, i.e. across domain boundaries and across grain boundaries (path A), or along grain boundaries only (path B) (see Fig. 7(b)).

The IBLC proposed by Sinclair et al. [5] cannot explain the high dielectric constant of single crystal CCTO. Therefore, some researchers proposed the idea of internal/twin domain boundary elements inside the grain as a possible solution [8,33]. Chung [37] and Fang and Liu [38] have observed polycrystalline specimens of CCTO using TEM and showed that the grains consist of domains and thick domain walls. Fang et al. [25] have also investigated the temperature-dependent resistivity of grain boundaries and domain boundaries, and confirmed the presence of domain boundaries and that their resistivity is lower than that of the grain boundaries.

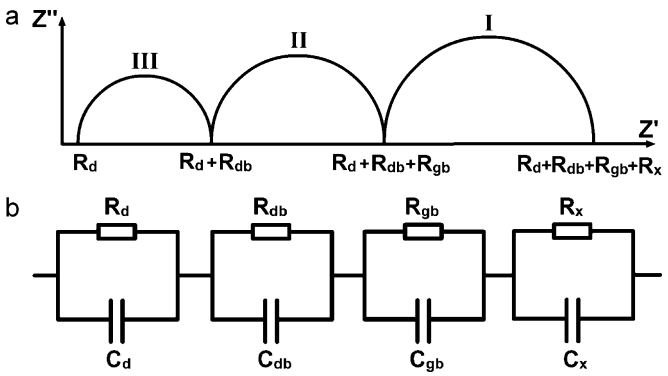

Fig. 6. Schematic impedance complex plane plot for three arc samples (a) and its equivalence *RC* circuit (b).

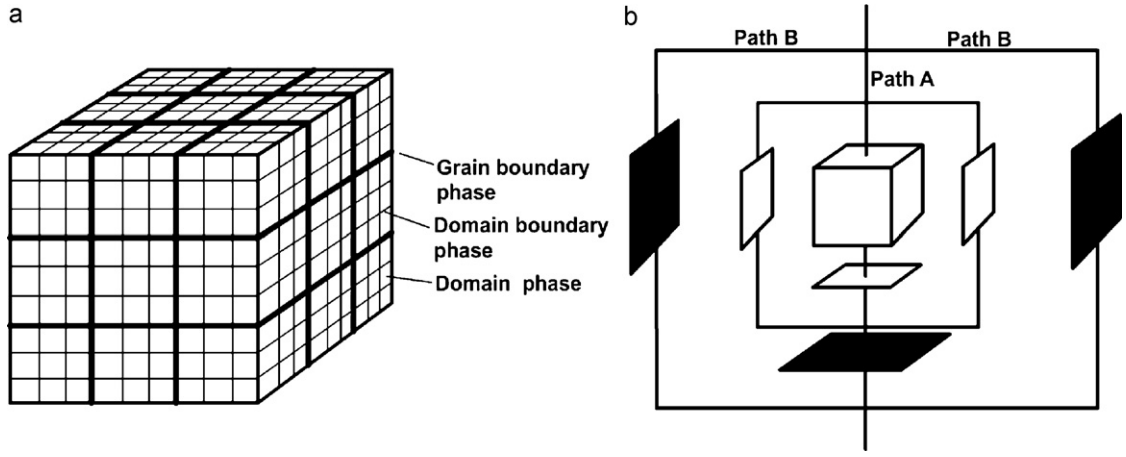

Fig. 7. Brick layer model for a three-phase ceramic: (a) overall view, showing array of cubic domains within cubic grains, separated by flat grain boundaries. (b) Exploded view of a single cell, showing parallel electrical paths: (i) through domain, domain boundaries and grain boundaries, and (ii) along grain boundaries.

In order to understand the phenomenon of the high frequency arc of impedance complex plane, this current work investigated the domain resistance, R_d and domain boundary resistance, R_{db}. It is suggested that the high frequency arc originated from R_d and R_{db}. From the IS measurement, the R_d for all samples is very low (conductive, about 1 Ω) and the fitting curve of the impedance complex plane for the domain boundary is approximately the same as the grain resistance, R_g. According to the IBLC model, there is a conductive grain with an insulating barrier of grain boundary. Later, it was found that another type of insulating barrier known as the domain boundary contributes to the "giant dielectric phenomenon" [24,25,38,39]. At high frequencies (>10 MHz), the effect of grain boundary resistance is no longer dominant as the dielectric constant of CCTO ceramic drops rapidly, but the domain boundary effect remains. Based on our previous findings about the dielectric constant of Nb-doped CCTO [21], the dielectric constant of CCTO samples at high frequencies are strongly dependent on the domain boundary resistance. Domain boundary resistance is inversely

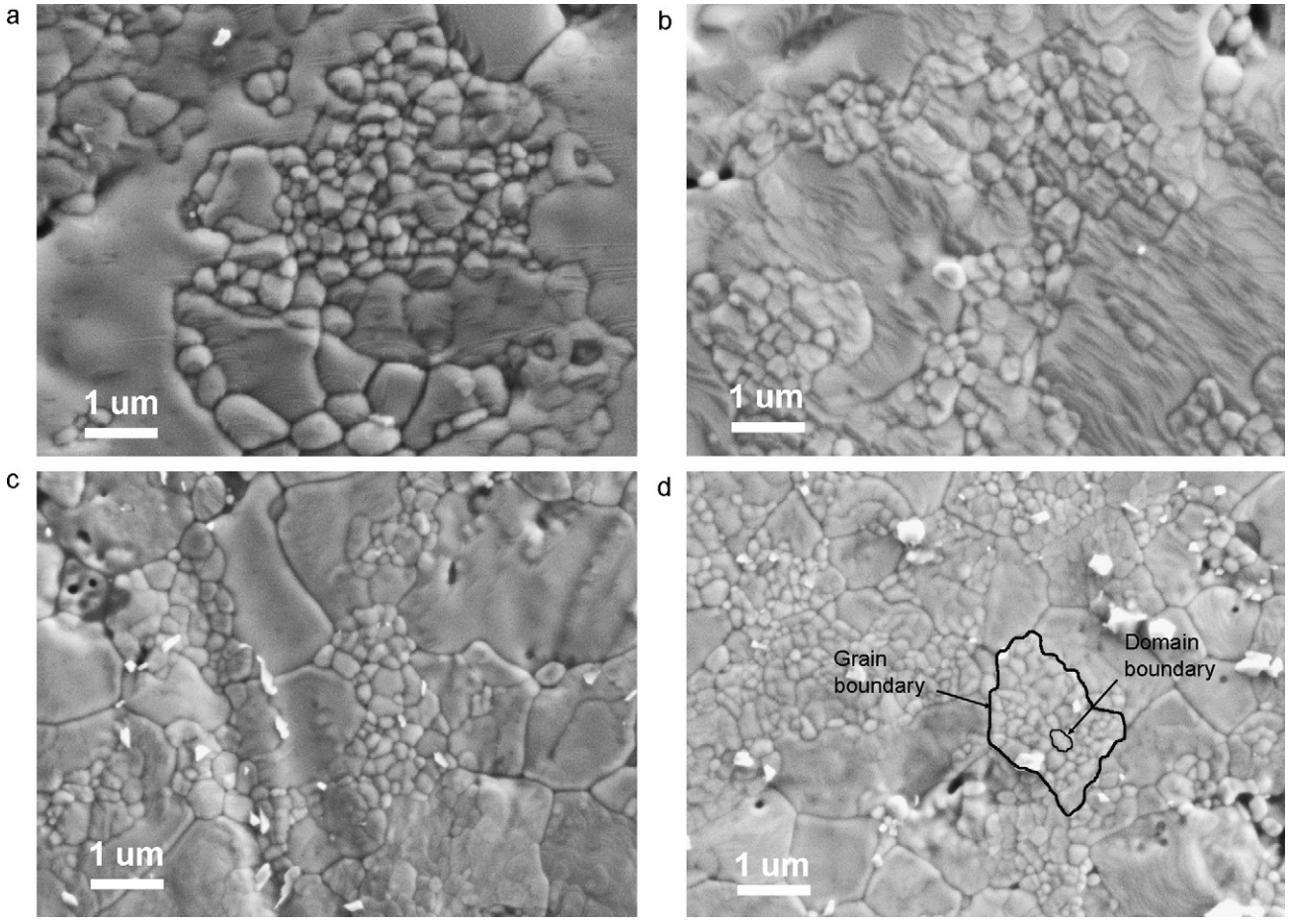

Fig. 8. FESEM micrographs for the thermally etched of pre-sintered Nb-doped CCTO ($CaCu_3Ti_{4-x}Nb_xO_{12+x/2}$) pellets: (a) undoped pellet ($x = 0$), (b) doped with 1 mol% Nb ($x = 0.01$), (c) doped with 5 mol% Nb ($x = 0.05$), and (d) doped with 10 mol% Nb ($x = 0.10$).

Table 1
The resistivity of domain, grain and grain boundary of $CaCu_3Ti_{4-x}Nb_xO_{12+x/2}$ ceramics.

x	R_d (Ω)	R_{db} (Ω)	R_{gb} (MΩ)	R_x (MΩ)	ε (0.1 GHz)	ε (1 GHz)
0.00	0.91	109	33.5	–	218	224
0.01	1.09	27	4.3	–	423	437
0.03	1.14	43	7.3	–	322	286
0.05	0.99	23	0.7	1.5	524	567
0.10	1.14	44	0.1	2.9	398	274

proportionate to the dielectric constant, as shown in Table 1. This assumption is in agreement with other researchers who also measured CCTO samples at high frequencies [20,24,34].

Fig. 8 shows the FESEM micrographs of pre-sintered $CaCu_3Ti_{4-x}Nb_xO_{12+x/2}$ pellets thermally etched at 940 °C for 1 h. Large grains and thick grain boundaries can be seen with small domains distributed inside the grains for samples $x = 0$ and 0.01 (Fig. 8(a) and (b)). The size of the grain boundary is reduced with the increase of doping concentrations, i.e. $x = 0.05$ and 0.10 as shown in Fig. 8(c) and (d). The average grain and domain sizes were measured statistically using SEM images. The effect of dopant to the grain as well as domain size is shown in Fig. 9. Both curves of the grain and domain exhibit a similar trend where the size decreased when dopant concentration was increased. Moreover, SEM micrographs in our previous work indicated that the increment of doping concentrations in Nb-doped CCTO will change the abnormal grain growth to normal grain growth, i.e. finer grain [21]. This phenomenon usually happens when CCTO is doped with a donor dopant because the excess electrons tend to reduce the concentration of oxygen vacancies. Oxygen vacancies can exchange themselves with neighbour oxygen ions to promote ion mobility and is expected to be a cause of abnormal grain growth. Therefore, the decrease in grain size is also closely linked to inhomogeneous distribution of oxygen vacancies between lesser oxygen deficient surfaces and the more oxygen deficient surfaces of high dopant concentration samples [35].

The relationship between the impedance complex plane and microstructure is thus clearly revealed. Samples with two semicircles have larger grain size and thicker grain boundary, as shown in Fig. 8(a) and (b), compared to samples with three semicircles which have fine grain and thin grain boundary (Fig. 8(c) and (d)). The samples with thinner grain boundary (highly doped samples) have low grain boundary resistance (R_{gb}) of the impedance complex plane and high surface oxidation layer resistance (R_x) that appear at low frequency arc. On the other hand, the R_{gb} of samples with thicker grain boundary (lightly doped samples) is very high (Table 1). Therefore, the R_x cannot be detected on samples with thicker grain boundary as it overlaps with their R_{gb}. The grain interior of each of the samples contain many tiny domains in the form of bumps and terrace shapes and this can be related to the high frequency response of CCTO at the first semicircle in the impedance complex plane. Fang and Shia [39] also found the two kinds of domain morphologies and concludes that the finding solves the contradictions related to the interpretation of the giant dielectric response between ceramic and single crystal CCTO.

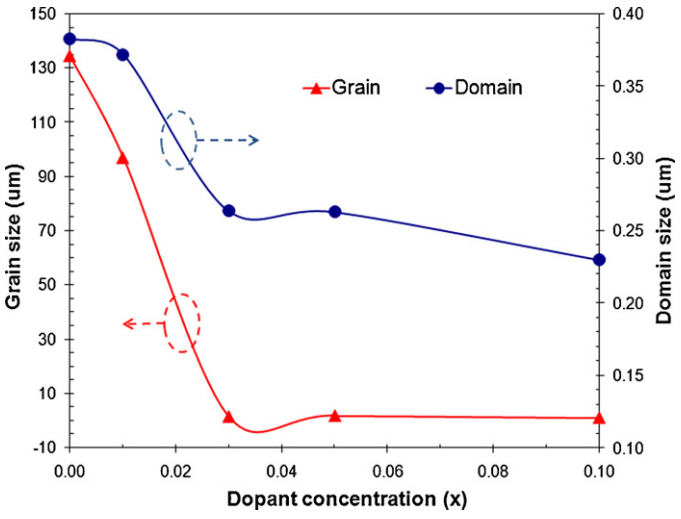

Fig. 9. Effect of dopant concentration on the grain and domain size of Nb-doped CCTO. The domain size was measured from the SEM micrographs of thermal etched at 940 °C/1 h of pre-sintered pellets.

4. Conclusions

Impedance spectroscopy measurement was performed on Nb-doped CCTOs. It was found that the conductive response at high frequency (1 MHz to 1 GHz) might have originated from domain elements inside the grains. The domain boundary resistance obtained from the high frequency fitting curve are approximately the same as the grain resistance itself. The grain resistance of CCTO is much lower compared to its grain boundary resistance. In this work, the existence of both domain and grain resistance are believed to strongly influence the dielectric constant of CCTO. These findings can be explained by the proposed model, where the large grains of CCTO consist of smaller cubic-shaped grains called domains. The domains are separated from each other by flat domain boundaries to form domain arrays inside the grain. As a grouped domain, the grains are also separated by flat grain boundary. This proposed model was supported by microstructure images which show a large grain and thick grain boundary with smaller grains (domains) distributed inside the grain.

Acknowledgment

The authors gratefully acknowledge that this work was financially supported by the Science Fund from the Ministry of Science, Technology and Innovation (MOSTI), Malaysia, under project no. 03-01-05-SF0432. M.A. Sulaiman wishes to thank Universiti Sains Malaysia for awarding him a PhD Fellowship Scheme.

References

[1] A.P. Ramirez, M.A. Subramanian, M. Gardel, G. Blumberg, D. Li, T. Vogt, S.M. Shapiro, Solid State Commun. 115 (2000) 217–220.
[2] J. Lu, D. Wang, C. Zhao, J. Alloys Compd. 509 (2011) 3103–3107.
[3] B.S. Prakash, K. Varma, J. Phys. Chem. Solids 68 (2007) 490–502.
[4] C. Wang, L. Zhang, Appl. Phys. Lett. 88 (2006) 042906.
[5] D.C. Sinclair, T.B. Adams, F.D. Morrison, A.R. West, Appl. Phys. Lett. 80 (2002) 2153.
[6] T.B. Adams, D.C. Sinclair, A.R. West, Adv. Mater. 14 (2002) 1321–1323.
[7] C. Homes, T. Vogt, S. Shapiro, S. Wakimoto, A. Ramirez, Science 293 (2001) 673.
[8] D. Fu, H. Taniguchi, T. Taniyama, M. Itoh, S. Koshihara, Chem. Mater. 20 (2008) 1694–1698.
[9] E. Barsoukov, J.R. Macdonald, Impedance Spectroscopy: Theory, Experiment, and Applications, 2nd ed., John Wiley and Sons, 2005.
[10] A.J. Moulson, J.M. Herbert, Electroceramics: Materials, Properties, Applications, 2nd ed., Chapman & Hall, London, 2003.
[11] F. Amaral, M. Valente, L. Costa, J. Non-Cryst. Solids 356 (2010) 822–827.
[12] P. Leret, M.A. de la Rubia, J.J. Romero, J.F. Fernandez, J. Am. Ceram. Soc. 93 (2010) 1866–1868.

[13] J.M. Golio, RF and Microwave Semiconductor Device Handbook, CRC, 2003.
[14] A. Almeida, R. Silva, H. Rocha, P. Fechine, F. Cavalcanti, M. Valente, F. Freire, R. Sohn, A. Sombra, Physica B 403 (2008) 586–594.
[15] A.K. Dubey, P. Singh, S. Singh, D. Kumar, O. Parkash, J. Alloys Compd. 509 (2011) 3899–3906.
[16] S.H. Hong, D.Y. Kim, H.M. Park, Y.M. Kim, J. Am. Ceram. Soc 90 (2007) 2118–2121.
[17] X.H. Zheng, C. Zhang, B.L. Liang, D.P. Tang, X. Huang, X.L. Liu, J. Alloys Compd. 505 (2010) L10–L14.
[18] S.D. Hutagalung, L.Y. Ooi, Z.A. Ahmad, J. Alloys Compd. 476 (2009) 477–481.
[19] S. Kwon, C.-C. Huang, M.A. Subramanian, D.P. Cann, J. Alloys Compd. 473 (2009) 433–436.
[20] P. Liu, Y. He, J.P. Zhou, C.H. Mu, H.W. Zhang, Phys. Status Solidi (a) 206 (2009) 562–566.
[21] M.A. Sulaiman, S.D. Hutagalung, M.F. Ain, Z.A. Ahmad, J. Alloys Compd. 493 (2010) 486–492.
[22] S. Jin, H. Xia, Y. Zhang, Ceram. Int. 35 (2009) 309–313.
[23] S. Kwon, C.C. Huang, E.A. Patterson, D.P. Cann, E.F. Alberta, W.S. Hackenberger, Mater. Lett. 62 (2008) 633–636.
[24] S.F. Shao, J.L. Zhang, P. Zheng, C.L. Wang, Solid State Commun. 142 (2007) 281–286.
[25] T.T. Fang, W.J. Lin, C.Y. Lin, Phys. Rev. B 76 (2007) 045115.
[26] S.D. Hutagalung, M.I.M. Ibrahim, Z.A. Ahmad, Mater. Chem. Phys. 112 (2008) 83–87.
[27] C. Homes, T. Vogt, S. Shapiro, S. Wakimoto, M. Subramanian, A. Ramirez, Phys. Rev. B 67 (2003) 92106.
[28] J.J. Mohamed, S.D. Hutagalung, M.F. Ain, K. Deraman, Z.A. Ahmad, Mater. Lett. 61 (2007) 1835–1838.
[29] S.Y. Chung, I.D. Kim, S.J.L. Kang, Nat. Mater. 3 (2004) 774–778.
[30] T.B. Adams, D.C. Sinclair, A.R. West, Phys. Rev. B 73 (2006) 1–9.
[31] M.C. Ferrarelli, D.C. Sinclair, A.R. West, H.A. Dabkowska, A. Dabkowski, G.M. Luke, Mater. Chem. 19 (2009) 5916–5919.
[32] B.S. Prakash, K.B.R. Varma, D. Michau, M. Maglione, Thin Solid Films 516 (2008) 2874–2880.
[33] D.L. Sun, A.Y. Wu, S.T. Yin, J. Am. Ceram. Soc. 91 (2008) 169–173.
[34] C. Mu, H. Zhang, Y. He, J. Shen, P. Liu, J. Phys. D: Appl. Phys. 42 (2009).
[35] Y. He, H. Zhang, P. Liu, J. Zhou, C. Mu, Physica B 404 (2009) 3722–3726.
[36] C.H. Mu, P. Liu, Y. He, J.P. Zhou, H.W. Zhang, J. Alloys Compd. 471 (2009) 137–141.
[37] S.Y. Chung, Appl. Phys. Lett. 87 (2005) 052901.
[38] T.T. Fang, C.P. Liu, Chem. Mater. 17 (2005) 5167–5171.
[39] T.T. Fang, H.K. Shiau, J. Am. Ceram. Soc. 87 (2004) 2072–2079.